Super-Resolution Imaging of Competitive Unlabeled DNA Hybridization Reveals the Influence of Fluorescent Labels on Duplex Formation and Dissociation Kinetics

Eric M. Peterson, Eric J. Reece, Wenyuan Li, and Joel M. Harris*

Department of Chemistry, University of Utah, 315 South 1400 East
Salt Lake City, Utah 84112-0850 USA

ABSTRACT

Single-molecule fluorescence imaging is a powerful method to measure reversible reaction kinetics, allowing one to monitor the bound state of individual probe molecules with fluorescently-labeled targets. In the case of DNA hybridization, previous studies have shown that the presence of a fluorescent label on a target strand can exhibit significant influence on the stability of DNA duplex that is formed. In this work, we have developed a super-resolution imaging method to measure *hybridization kinetics of unlabeled* target DNA that compete with a fluorescently-labeled tracer DNA strand to hybridize with an unlabeled probe DNA immobilized at a surface. The hybridization of an unlabeled DNA target cannot be detected directly, but its presence blocks the immobilized probe DNA, influencing the measured time intervals between labeled-DNA hybridization events. We derive a model for the competitive hybridization kinetics to extract the association and dissociation rate constants of the *unlabeled species* from the distribution of time intervals between hybridization events of the labeled-tracer DNA at individual localized DNA probe sites. We use this methodology to determine the hybridization kinetics of a model 11-mer unlabeled target DNA strand and then determine how five different fluorescent labels attached to the same target DNA strand impact the hybridization kinetics. Compared to the unlabeled target, these labels can slow the association and dissociation rates by as much as a factor 5. The super-resolution time-interval methodology provides a unique approach to determining fundamental (label-free) rates of DNA hybridization, revealing the significant influence of fluorescent labels on these kinetics. This measurement concept can be extended to studies of other reversible reaction systems, where kinetics of unlabeled species can be determined from their influence on the reaction of a labeled species with localized probe molecules on a surface.

* Corresponding author: harrisj@chem.utah.edu; phone: 801-581-3585

INTRODUCTION

Hybridization between small oligonucleotides control the behavior of systems in nanotechnology,[1] aptamer assembly,[2] genetics assays,[3] and gene regulation.[4] To understand the mechanism of these reactions and to better design their applications, experimental techniques are needed to measure the kinetics of oligonucleotide hybridization. There are a number of sensitive methods to measure hybridization between fluorescently-labeled oligonucleotides including fluorescence-resonance-energy transfer (FRET),[5] total-internal-reflection fluorescence,[6] and most recently, single-molecule fluorescence- and FRET-based imaging.[7-15] Fluorescence labeling has drawbacks, however, requiring ligation and purification of a labeled product, which is especially difficult for oligonucleotides extracted from biological samples. More importantly, labels can influence the energetics and kinetics of the intermolecular interactions themselves. Fluorescent nanoparticle labels (e.g. quantum dots or gold nanoparticles) decrease the diffusion rates of small oligos and interactions with the nanoparticle surface can alter hybridization kinetics.[16] Small organic fluorophores, such as Cy3 or rhodamine dyes, can interact strongly with nucleobases,[17-19] and these interactions can impact the stability of DNA duplexes.[5,20,21]

Label-free detection is needed to measure hybridization without the perturbations introduced by covalently-attached labels, but it is inherently challenging because nucleotides lack a chromophore that can provide comparable sensitivity as a well-designed fluorescent label. Traditional label-free techniques detect interfacial binding of molecules by a change in mass for quartz crystal microbalances,[22] changes in refractive index for surface-plasmon resonance,[23] or changes in local symmetry at the interface for sum-frequency or second-harmonic generation.[24] While useful for analytical applications, these techniques require high surface densities of probe molecules to capture sufficient target molecules to provide a detectable signal. High surface densities of probes can influence the measured binding kinetics by steric interactions,[25] by rebinding to nearby probe sites,[13] or, for systems with high binding affinity, by rate-limiting mass transport of target species from very dilute solutions to a high surface density of capture sites.[6,26-28]

Competitive-binding assays combine advantages of sensitive label-based sensing with the ability to measure the equilibrium constants of unlabeled species. In previous work from this lab, the hybridization between unlabeled target DNA and immobilized probe DNA could be measured in competition with a small fraction of fluorescently-labeled ‘tracer’ DNA that tracks

the population of available (unoccupied) DNA probe sites as they react unlabeled DNA.[21] The assay was performed using single-molecule imaging to count populations of hybridized labeled tracer DNA at equilibrium, while varying the solution concentrations of unlabeled DNA. Association constants for hybridization to an immobilized probe DNA were compared for identical DNA target strands differing only by the addition of a fluorescent label, which was found to stabilize the resulting duplex by 3.6 $kJmol^{-1}$, an energy comparable to adding a adenine-thymine base-pair to the sequence.[21] While this equilibrium competition experiment is useful in determining the influence of a fluorescent label on DNA association constants compared to unlabeled DNA, the association and dissociation *kinetics* of the unlabeled target DNA could not be determined from the average bound population of labeled 'tracer' DNA.

Using a super-resolution single-molecule fluorescence imaging technique called DNA point-accumulation-imaging-of-nanoscale-topology (DNA-PAINT),[7,29] one can localize and address individual immobilized DNA probe molecules on a surface. This approach can determine DNA hybridization kinetics between fluorescently-labeled DNA molecules in solution and *individual immobilized probe DNA molecules*, simultaneously tracking the hybridization state of many localized probe molecules on a surface.[7,12,13,29,30] This technology can allow one to detect the presence and influence of non-fluorescent molecules on site-selected kinetics of fluorescent molecules, as shown in recent research that used super-resolution imaging to locate catalytic sites for the generation of a fluorescent product: by knowing the locations of these sites, non-fluorescent reactions that compete for access to a catalytic site can be observed.[31] In the present work, we employ this same concept, using super-resolution imaging of hybridization of labeled DNA 'tracer' to locate individual DNA probe molecules on a surface and monitor the influence of *unlabeled target DNA* on the hybridization of the labeled tracer. The time intervals between hybridization events of the labeled tracer are sensitive to competition with unlabeled target DNA. When unlabeled target DNA hybridizes with an immobilized probe strand, it blocks the site thereby preventing hybridization with the labeled tracer DNA. The unlabeled target alters the distribution of time intervals between labeled-tracer DNA hybridization events, with a time response that is sensitive to both association and dissociation rates of the unlabeled target strand. A differential rate model of the competitive hybridization kinetics is derived and verified with Monte-Carlo simulations and then used to extract hybridization rate constants of unlabeled target species in competition with a labeled-DNA tracer. We compare the hybridization kinetics of the

unlabeled target strand to those of equivalent target DNA strands having one of several covalently attached labels: Cy3, PEG-tethered Cy3, dsDNA-tethered Cy3, carboxytetramethylrhodamine (TAMRA), and Alexa Fluor 532 (Figure S1). Since the kinetics are measured using the same substrates, immobilized probes, and instrumentation, we can compare the kinetics of labeled and unlabeled species without artifacts or bias from using different methods for label-based versus label-free detection. Our results show that the fluorescent labels significantly impact hybridization association constants by factors of 0.3 to 3.5 compared to an unlabeled strand and that underlying changes to association and dissociation rates vary significantly with the structure of the fluorescent label and with the tether used to attached it to the target DNA strand.

EXPERIMENTAL SECTION

Oligonucleotides and buffers for hybridization experiments. DNA was produced by both the University of Utah HSC Core DNA synthesis facility using solid-phase phosphoramidite chemistry with reagents from Glen Research and Biosearch, and by IDT with reagents from Thermo Scientific. DNA samples with a covalently-attached fluorescent labels were HPLC purified, while all other oligonucleotides were cartridge-purified. The DNA sequences used include the "capture" strand synthesized with a 3' alkyl-amine modification for covalent-coupling to the glycidyloxysilane surface, with a repeating sequence: 5'-$(AC)_9$-3'-NH_2. "Probe" DNA strands contain a repeating "GT" segment complementary with the capture sequence to allow capture at the surface, along with a target-recognition sequences: 5'-$(GT)_9$ TTC GGT ATA TCC CAT. The "unlabeled target" DNA strand is complementary with the last 11 base pairs of the probe DNA: 5'-ATG GGA TAT AC. The DNA sequences of "labeled targets" have the same sequences as the "unlabeled target", but with several different fluorescent labels (Figure S1) attached to the 5' end as shown in Scheme 1. "Tracer" DNA has a 5' PEG-linked Cy3 dye and shares sequence overlap with the labeled target, but has two nucleotides removed from the 3' end: Cy3-$(PEG)_6$-5'-ATG GGA TAT to allow faster exchange. Hybridization experiments were carried out in sodium phosphate buffer solutions, 15 mM phosphate at pH 8.0, with 200 mM sodium chloride supporting electrolyte.

DNA capture substrate preparation. DNA hybridization substrates were prepared on glass coverslips (Corning Gold Seal, Thermo Scientific). Coverslips were rinsed with ultrapure water (GenPure UV) three times and then cleaned with acid piranha solution for 20 minutes: 1:3

30% hydrogen peroxide: 96% sulfuric acid (caution: corrosive, strong oxidizer, reacts explosively with organic solvents). Coverslips were then rinsed with ultrapure water three times and cleaned with RCA base bath[32] at 70°C for 20 minutes: 1:1:5 30% hydrogen peroxide solution: 30% ammonium hydroxide solution: ultrapure water. Coverslips were rinsed with ultrapure water and dried at 120°C for 30 minutes, before being cooled to 80°C for 10 minutes. Slides were then sealed in a jar containing a vial with 250-μL of 3-glycidoxypropyl-trimethodxysilane and placed in an 80°C oven for 90-120 minutes to deposit a uniform silane layer on the glass with few defect sites.[33,34] Substrates were then removed from the deposition chamber and placed in a 120°C oven for 90 minutes to drive off unreacted silane and promote cross-linking of the trifunctional silane layer.

After the oven treatment, 3'-amine-modified capture DNA was immobilized on the glycidoxy-modified glass coverslips by placing a 15 μL droplet of 100 μM capture DNA in 100-mM pH-10.0 sodium-carbonate buffer on a coverslip. Another coverslip is placed on the first to squeeze the droplet into a thin film to maximize surface coverage of the coverslip while minimizing the reaction volume. Coverslips were placed in a 40°C oven for 4-12 hours to allow immobilization of capture DNA and then rinsed with ultrapure water. Coverslips were then placed in a solution of 20 mM 3-amino 1-propanesulfonic acid in 100 mM pH 10.0 carbonate buffer for 8 hours at 40°C to passivate unreacted glycidoxy groups. Substrates were then rinsed in water and stored in ultrapure water for up to 14 days at 2°C before use.

Fluorescence microscopy and image acquisition. DNA-modified coverslips were sandwiched into a microfluidics flow cell comprising a top-plate with inlet and outlet ports and thin double-stick tape gasket material (3M 9495MP), as described previously.[21] Hybridization between probe and fluorescently-labeled target DNA was monitored at the coverslip-solution interface using an Olympus IX-71 inverted microscope with objective-based TIRF illumination.[30] A fiber-coupled 532 nm laser (BWTek) was used as an excitation source. Light from the fiber was collimated by an achromatic doublet lens (Thorlabs), passed through an aperture to control beam diameter, sent through a quarter wave plate (Thorlabs), a shutter (Uniblitz), reflected from a dichroic mirror (Semrock), and focused with an achromatic doublet (Thorlabs) onto the back-focal plane of the microscope objective (60x, 1.45NA, Olympus). The focus is translated off the center-axis of the objective to produce a collimated excitation beam that is internally-reflected at the sample-solution interface. Fluorescence from the sample is

collected by the objective and sent through the dichroic mirror, emission filter (Semrock), and a 1.6x magnifier and imaged on the CCD detector. The temperature of the microscope system and sample was controlled by enclosing the microscope in a fiberboard cabinet and using a proportional-integral-derivative controlled heater-fan assembly (Omega HVL14900) to maintain temperature at 27.1±0.1°C monitored by a NIST-traceable thermometer (VWR).

Fluorescence images were collected using an Andor iXon DU897 electron-multiplying charge-coupled device camera with exposure times designed to minimize photobleaching while still sampling the hybridization kinetics. Tracer hybridization for the 9-mer labeled target was monitored in either continuous videos with 200ms exposure times, or time-lapse videos with 100 ms exposures and 300-ms intervals. The total laser energy exposure experienced (37.5 or 23.9 Wcm^{-2} during exposures) by the Cy3 fluorophores is comparable to previous work from this lab, where we observed minimal influence of photobleaching on the measured dissociation rate.[30] For the present experiments, we find that increasing the excitation intensity by 50% has no detectable influence on the 9-mer dissociation rate. For the longer-lived 11-mer labeled targets (Alexa Fluor, TAMRA, Cy3, PEG-Cy3, dsDNA-Cy3), we collect images on longer (2-4s) time-lapse intervals, and additionally, for the Cy3 and Alexa Fluor duplexes, we employ an oxygen-scavenging enzyme buffer to reduce photobleaching and photoblinking[35-38] (Supporting Information). The kinetics of Cy3-labeled targets were found to have the greatest sensitivity to oxygen-dependent photobleaching. With oxygen scavenging, the impact of photobleaching on the measured rate of the Cy3-labeled 11-mer target dissociation is small, ~1% (Figure S2). All images were collected in a 300x300 pixel area of the CCD, corresponding to 50x50μm in the sample plane. The camera was operated without electron-multiplying gain at slow 1MHz readout to avoid photoelectron-amplification noise and minimize read noise.[39] Images were acquired as 10-40 min 16-bit monochrome FITS-image stacks with Andor SOLIS software 4.27.30001.0.

Image Analysis. To analyze these images, an intensity-threshold algorithm[40] was used to locate individual molecules which accounted for the spatial distribution of intensity background due to the high concentration of labeled DNA in the evanescent wave.[30] Each single-molecule point-spread-function was fit to a 2D Gaussian function to locate its position. Sample drift is corrected by performing a spatial-temporal cross-correlation analysis of all located molecule coordinates.[12] Drift-corrected super-resolution molecular coordinates were tracked within a generous detection radius of 80 nm in subsequent image frames to measure labeled-molecule

residence times. Each individual single-molecule "event" is then used to locate probe sites and measure hybridization kinetics. Details are in Supporting Information.

RESULTS AND DISCUSSION

Kinetics of fluorescently-labeled tracer DNA hybridization. To immobilize probe DNA at the interface, a mixture of 200 pM probe and 30 nM tracer DNA is injected over a slide-with immobilized AC-repeat capture DNA, while monitoring the population of tracer DNA at the interface (Scheme 1). Probe DNA is captured by its complementary GT segment, while Cy3-labeled tracer DNA hybridizes with the recognition region of the probe DNA allowing the population of captured probe to be monitored in real-time with fluorescence microscopy. Once the population of probe-tracer duplexes reaches a desired surface density, probe-accumulation is terminated by rinsing the cell with buffer for 10-15 minutes removing tracer DNA along with unbound or partially hybridized probe DNA. A solution of 30-nM tracer DNA can then be reinjected into the flow cell to allow imaging of its hybridization with the immobilized probe DNA, Figure 1B. This result is compared with a blank measurement where 30-nM Cy3-labeled tracer DNA is introduced prior to immobilization of probe DNA, producing an average of 15±5 molecules per image (Figure 1A), which is 3% of the 470±30 hybridized tracer DNA molecules observed with probe DNA immobilized (Figure 1B).

Fluorescence videos of probe substrates in equilibrium with 30-nM tracer DNA in solution show transient single-molecule binding events occurring at discrete probe molecule sites (Supporting Information). We track individual tracer hybridization events that appear in tight clusters at each probe molecule using super-resolution localization,[41] and these drift-corrected molecule coordinates are plotted as a 2D histogram map (Figure 1B inset). The size of the clusters of hybridization events around immobilized probes is determined by the localization precision (~40 nm).[30] In contrast, substrates with no immobilized probe DNA exhibit sparse maps of dispersed tracer DNA adsorption events with a few clusters suggesting sites of stronger nonspecific adsorption (Figure 1A inset).

Locations of probe DNA molecules are identified by requiring a minimum of 3 hybridization events within an 80-nm radius, which rejects spurious adsorption sites, more than half of which produced only a single event. Probe sites were also discarded if they were closely spaced (within 160 nm) in order to prevent cross-talk between adjacent probes that might skew the hybridization statistics. Based on these criteria, we identify ~5200 immobilized probe

molecules within a 50μm-by-50μm area, at which a total of 69,000 hybridization events are observed in 5 min with 30-nM tracer. With no probe DNA immobilized, the same substrate exposed to the same tracer DNA concentration produced only 56 sites that meet the same criteria, indicating only ~1% of the identified probe molecule sites are a result of nonspecific interactions. Of the approximately 7000 nonspecific adsorption events observed in a blank data set, only about 5% appear at specific surface locations while remaining 95% are at random, uncorrelated (single-event) locations on the surface. Restricting our observation to 5200 probe sites, each having an 80-nm detection radius, the total detection area is ~4% of the field-of-view. By confining the observation to this limited area, only ~280 of the 7000 nonspecific adsorption events would randomly land on a probe site, contributing a negligible 0.4% of the hybridization events at probe sites. Imposing super-resolution spatial criteria on the interrogation probe-molecule hybridization, therefore, *greatly improves the selectivity* of measurement by reducing the impact of non-specific adsorption.[30,42,43]

After restricting the analysis of hybridization events to spatially-resolved probe molecule sites, histograms of the durations and time intervals between hybridization events can be generated, shown in Figure 2. These histograms are plotted as cumulative survival histograms, so that the quantity in each bin represents the number of events that survived at least that amount of time.[44] The histograms are fit well by a single-exponential decay probability function (Equation 1), characteristic of first-order dissociation and pseudo first-order association kinetics:

$$p(t) = N\exp(-t/\tau) \qquad (1)$$

where τ represents the average association or dissociation lifetime, τ_{on} or τ_{off} respectively, and N represents the total number of hybridization events.

To assess the uniformity of the kinetics amongst the population of probe molecules, the distributions of association and dissociation lifetimes at each *individual* probe molecule are determined from a maximum-likelihood estimate (MLE) of the mean of an exponential distribution,[45] with an offset to subtract bias from the duration of the first sampled time-bin, *j*:[30]

$$\tau^{MLE} = \left(\frac{T}{N}\sum_{i=j}^{i=\infty} i\, n_i\right) - T(j - 1/2) \qquad (2)$$

where T is the bin width, N is the total number of events, and n_i is the number of events in bin i. Analysis of the 5-20 hybridization events sampled at each probe molecule, distributions of maximum-likelihood association and dissociation lifetimes over the population of probe-molecules are plotted in the insets of Figure 2. These distributions are well described by a

Poisson-Erlang (PE) distribution[30,46] which predicts the distribution of *k*-lifetime samples drawn from an exponential distribution (Supporting Information, Equation S1). The width of the PE distribution is determined by the average number of sampled events (more samples result in tighter distributions) plus any heterogeneity in lifetimes as a result of molecule-to-molecule variability. Comparing the standard deviation predicted by sampling statistics (Equation S2) with the standard deviation of the measured lifetime distributions, we find ≤ 20% excess width of the experimental distributions (Supporting Information, Table S1). The impact of this excess lifetime variation on determining the hybridization kinetics is negligible, as discussed below.

Modeling hybridization kinetics with unlabeled competitors. Having determined that reversible hybridization between probe and labeled-tracer DNA is well described by homogeneous first-order kinetics, a model can be developed for the microscopic rates governing hybridization in the presence of an unlabeled competitor, as shown in Figure 3A. The solution species in the model and their concentrations are the labeled-tracer, [*L*], and unlabeled-target DNA, [*U*]. These species compete to hybridize with free probe DNA molecules, [*P*], generating probes that are hybridized with either labeled-tracer, [*LP*] or with unlabeled-target, [*UP*], respectively. In this model, target and tracer DNA from solution only hybridize with unoccupied probe DNA [*P*], that is, they do not displace each other. This assumption is reasonable, since the 11-mer unlabeled-target is only 2 base-pairs longer than the 9-mer labeled-tracer, so that the rate of toe-hold strand displacement should be negligible.[47] This hypothesis was confirmed by observing *no detectable dependence* of the dissociation rate of the labeled tracer with concentration of the unlabeled 11-mer target (see below and Supporting Information, Figure S5). Upon dissociation of either labeled-tracer or unlabeled-target from a probe molecule, the probe returns to the unbound state, [*P*]. The sum of the concentrations of all probe species is equal to the total number of probe sites: $[P_{tot}] = [P] + [UP] + [LP]$. We define first-order rate constants for dissociation of labeled tracer and unlabeled target DNA, k^o_{offl} and k^o_{offu}, and second-order rate constants for association with probe DNA from solution, k^o_{onl} and k^o_{onu}, respectively.

Monte-Carlo simulations were employed to explore how probe DNA hybridization with unlabeled target DNA affects the *time intervals* between tracer hybridization events, and whether these hybridization intervals can be used to determine the rate constants of the unlabeled target DNA hybridization. The simulation tracks the state of a probe DNA molecule undergoing competing hybridization with tracer and target DNA. The lifetime of each hybridized state is

determined by a random time drawn from an exponential probability distribution with a characteristic rate constant, k:

$$p(t;k) = kexp(-kt) \quad (3)$$

As shown above in Figure 2, this is a reasonable model for hybridization dissociation kinetics. Dissociation times are drawn from either labeled-tracer or unlabeled-target distributions, governed by their respective rate constants, k^o_{offl} or k^o_{offu}. Association times for labeled tracer and unlabeled target, which compete to hybridize with available probe sites, [P], are drawn from exponential distributions with rates: $k_{onl} = k^o_{onl}[L]$ and $k_{onu} = k^o_{onu}[U]$, respectively, where the faster rate determines which species generally hybridizes first. Monte-Carlo simulations (Supporting Information) were run to generate 17,000-70,000 tracer hybridization events using input rate constants similar to those expected for the tracer and target DNA. A constant tracer concentration is assumed, so that the quantity $k_{onl} = k^o_{onl}[L]$ is not varied, and the dissociation rates, k_{offl} and k_{offu}, also do not change with concentration. The unlabeled-target association rate $k_{onu} = k^o_{onu}[U]$ is varied to simulate an experiment conducted with varying unlabeled target concentrations. From these simulated trajectories, we predict time intervals between tracer molecules leaving and a new tracer molecule arriving as a function of [U]. Histograms of association-time intervals from these simulations, along with the input rate parameters, are plotted in Figure 3B. By increasing the association rate of an unlabeled target, the association-time-interval distributions deviate significantly from a single-exponential decay profile and exhibit short-lived and long-lived components, the relative magnitudes and lifetimes of which vary with k_{onu}.

To extract rate constants from these distributions, we model this competing hybridization process as a pair of differential equations describing the change in population of occupied and unoccupied probe molecules. The hybridization interval distributions are analogous to a concentration-step experiment, where all probe molecules are initially unoccupied with tracer or target DNA.[48] This initial condition represents the state of the probe immediately after a tracer molecule dissociates and establishes time-zero for the measurement of an interval between hybridization events. Unlabeled-target or labeled-tracer DNA can then hybridize with the unoccupied probes, and we monitor the probe while it is *not* hybridized with tracer DNA, [UP] + [P] until the interval ends, when a new fluorescent tracer DNA hybridizes with the probe. The dissociation rate of the tracer does not affect the time intervals between tracer association events

and is not included in the model. A pair of differential equations describes the change in population of unoccupied probes (4) and probes hybridized with unlabeled target (5) following dissociation of the labeled tracer:

$$\frac{d[P]}{dt} = -k^o_{onu}[U][P] + k^o_{offu}[UP] - k^o_{onl}[L][P] \quad (4)$$

$$\frac{d[UP]}{dt} = k^o_{onu}[U][P] - k^o_{offu}[UP] \quad (5)$$

We solve this system of differential equations for the time-evolution of [P(t)] + [UP(t)], using the boundary conditions [P(0)] = P_{tot}, [UP(0)] = 0, and [LP(0)] = 0. The solution can be represented by the sum of two exponential decay functions with decay rates, k_1 and k_2, and pre-exponential factors, A_1 and A_2, which are functions of the hybridization rates, k_{onu}, k_{offu}, and k_{onl}:

$$P(t) + UP(t) = P_{tot}[A_1 e^{k_1 t} + A_2 e^{k_2 t}] \quad (6)$$

where:

$$k_1 = \frac{k_{offu}+k_{onl}+k_{onu}+k_q}{2} \quad (7)$$

$$k_2 = \frac{k_{offu}+k_{onl}+k_{onu}-k_q}{2} \quad (8)$$

$$A_1 = \frac{k_{onl}-k_{offu}-k_{onu}+k_q}{2k_q} \quad (9)$$

$$A_2 = \frac{k_{onl}-k_{offu}-k_{onu}-k_q}{2k_q} \quad (10)$$

$$k_q = \sqrt{k^2_{offu} + k^2_{onl} + k^2_{onu} - 2k_{offu}k_{onl} + 2k_{offu}k_{onu} + 2k_{onl}k_{onu}} \quad (11)$$

This time-response function for the tracer hybridization intervals, Equation 6, can be fit to the simulated intervals in Figure 3B to extract the rate parameters to compare with those used to seed the simulation. For the fit to be sensitive to the initial fast exponential decay (represented by a smaller number of points), the squared residuals were weighted by t^{-1} in the minimization. The simulation and fitting routine were run 5 times to estimate uncertainties, and the rate parameters from the fit match the seeded rate constants within their uncertainties (Figure 3B inset). To confirm the rate parameters are unique solutions, we performed a covariance analysis by systematically varying one rate constant and floating the others in the least-squares fit. This analysis shows that if the value of one rate is changed, then the other rates cannot be varied to compensate without significantly reducing the quality of the fit, showing that the rates are independent and the solution is unique (Supporting Information, Figure S6). As discussed above,

individual immobilized probe molecules exhibit a distribution of hybridization association times having a ~20% excess standard deviation compared to the uncertainty predicted by sampling statistics. The influence of this excess error was tested by introducing 20% normally-distributed variation in the hybridization rates used to seed the Monte-Carlo simulations above. The additional error did not significantly impact the extracted parameters from a fit of Equation 6, where the unlabeled target association and dissociation rates at higher [U] exhibited less than 2% relative error compared to their seeded values (Supporting Information, Table S2).

Competitive hybridization experiments. Having developed and qualified a method to extract the kinetics of unlabeled target strand hybridization from the analysis of time intervals between tracer-DNA hybridization events, we apply this method to interpret experimental data of competitive hybridization between 11-mer unlabeled-target and 9-mer labeled-tracer DNA. Competitive hybridization was measured at individual immobilized probe DNA molecules using solutions of varying unlabeled target (5-100 nM) and fixed tracer DNA (30 nM) concentration. At high concentrations of unlabeled target DNA (50-100 nM), probes are occupied with unlabeled target more than 75% of the time, which slows the tracer hybridization on-rate. To collect sufficient tracer hybridization events to characterize the hybridization interval distribution at high unlabeled target concentrations, the length of image acquisition is increased from 5 min to 27 min. After data from all unlabeled target concentrations were acquired, the flow cell was rinsed and a solution of pure 30-nM tracer DNA was imaged to locate all the probe molecule coordinates in the field of view. These probe sites are filtered to exclude a ~5% fraction whose tracer-DNA kinetics falls well outside the Poisson-Erlang distribution, providing a homogeneous population of probe sites for testing competitive hybridization. The 95% remaining probe sites are used to fix coordinates to record hybridization events at individual probe molecules versus unlabeled target DNA concentration. The resulting hybridization event distributions (Supporting Information, Figure S7) reveal a small (12%) population of sites whose numbers of tracer events are unaffected by high concentrations of unlabeled target. These probe sites exhibit similar hybridization events as expected for solutions containing only tracer DNA, indicating that the unlabeled target does not hybridize with this population of probe molecules. This may be due to damage at the guanine or adenine bases needed to pair with the 3’ end of the longer unlabeled target, or interactions between the probe DNA and the surface or capture strand that prevent duplex formation with the longer unlabeled target. Regardless of their origins, these probe sites

are *at known locations* and easily excluded from the analysis, which can be deployed on the 88% of sites that demonstrate a competitive response to the unlabeled target. The ability to deal with site-dependent heterogeneity in the analysis of single-molecule kinetics is a clear benefit of imaging and analysis of interactions with individually-addressed molecular probe sites over ensemble methods, where site heterogeneity cannot be resolved or mitigated.[30,42]

The association and dissociation times for the probe sites that respond to the unlabeled target were pooled and plotted as survival-time histograms. The dissociation-time histograms and fitted rates show no detectable dependence on the unlabeled competitor concentration (Supporting Information, Figure S5), which verifies that competitive hybridization does not affect the stability and lifetime of the probe-tracer duplex. This confirms the assumption made in development of the competitive model that a 2-base-pair overhanging region on the unlabeled target is insufficient to induce toe-hold strand displacement that would shorten the tracer-duplex lifetime. Unlike tracer dissociation times, the time-intervals *between* tracer hybridization events increase significantly at higher unlabeled-target concentrations, as probe molecules are occupied by the competitive unlabeled target DNA and unavailable for tracer hybridization. Association times are plotted as histograms in Figure 4A, with examples shown for 0-, 20-, and 100-nM unlabeled target DNA.

To extract rate parameters for target and tracer hybridization, Equation 6 was fit to the data in Figure 4A, where the bi-exponential models that best fit the data are plotted as solid lines. The rate parameters from the interval-time model, k_{onl}, k_{onu}, and k_{offu}, were determined from four independent data sets, and the resulting association and dissociation rates of *the unlabeled 11-mer target* and their uncertainties are plotted in Figure 4B-C. The results show that the dissociation rate of the unlabeled target is independent of its concentration, consistent with unimolecular dissociation of the target-probe duplex, resulting in an average, k^o_{offu} = 0.032±0.001 s^{-1} (Figure 4B). The association rate of the unlabeled target, k_{onu}, increases linearly with target concentration with a zero intercept (Figure 4C), corresponding to a pseudo-first-order reaction; the slope of the line is the association rate constant of the unlabeled 11-mer target, k^o_{onu} = 1.74 (±0.02) x 10^6 $M^{-1}s^{-1}$, which is comparable to that of the 9-mer tracer, k^o_{onl} = 1.48 (±0.04) x 10^6 $M^{-1}s^{-1}$, which is also a parameter extracted from the data in Figure 4A.

The validity of these results can be checked in several ways. First, the kinetics of the tracer association and dissociation versus tracer concentration were measured in the absence of

the competitive unlabeled target. The results (Supporting Information, Figures S8 and S9) show that the tracer dissociation rate is independent of its solution concentration, consistent with a simple first-order process, exhibiting a 25-fold faster dissociation rate (k^o_{offl} = 0.79±0.02 s^{-1}) compared to the unlabeled 11-mer target strand, whose two additional base-pair interactions adds significant stability. The association rate of the labeled tracer DNA is linear with its concentration in solution (Supporting Information, Figure S9) and the rate constant determined from the slope, k^o_{onl} = 1.58 (±0.04) x10^6 $M^{-1}s^{-1}$, is within the uncertainties of the value found from the above competitive analysis, k^o_{onl} = 1.48 (±0.04) x10^6 $M^{-1}s^{-1}$. To further validate the hybridization rate constants of the unlabeled strand from the competitive hybridization model, we compare the association constant K_a determined from the ratio of rate constants with K_a determined from a competitive hybridization isotherm at equilibrium. Since the tracer is only able to hybridize with unoccupied probe molecules, it provides information about *the fraction of probe sites hybridized with unlabeled target DNA*, allowing determination of its K_a.[21] We calculate the fraction of time the probes are hybridized with tracer directly from the occupied and unoccupied lifetimes of each probe molecule. The fraction occupied is given by the ratio of maximum-likelihood-estimated (MLE) dissociation lifetimes of each probe molecule i, $\hat{\tau}_{off,i}$ from Equation 2, divided by the sum of the MLE association and dissociation lifetimes, $\hat{\tau}_{on,i}$, and $\hat{\tau}_{off,i}$, averaged over all probe molecules, N:

$$\theta([U]) = \frac{1}{N}\sum_{i=1}^{i=N} \frac{\hat{\tau}_{off,i}}{\hat{\tau}_{off,i}+\hat{\tau}_{on,i}} \qquad (12)$$

The resulting fraction hybridized with tracer DNA at each unlabeled target concentration is plotted in Figure 4D. Since the tracer occupies a significant fraction of the probe sites in the absence of unlabeled target (~6%), the equilibrium model includes hybridization of the probe by both tracer and target DNA. The expression for $\theta_L([U])$ thus depends on the labeled tracer concentration and its association constant, $K_L = k^o_{onl}/ k^o_{offl}$ = 2.0±0.1 μM^{-1} see above, as well as the association constant and concentration of the unlabeled target, K_a and $[U]$,

$$\theta_L = \frac{K_L[L]}{1+K_L[L]+K_a[U]} \qquad (13)$$

which is derived in Supporting Information, Page S16. A nonlinear least squares fit of Equation 13 to the equilibrium response in Figure 4D gives K_a = 60±10 μM^{-1}. K_a determined from measured rate constants above, $K_a = k^o_{onu}/k^o_{offu}$ = 54±4 μM^{-1}, matches the equilibrium result

within their uncertainties, indicating that the competitive kinetic results are consistent with the equilibrium response.

Impact of dye labeling on DNA hybridization kinetics. With knowledge of the hybridization kinetics of unlabeled DNA strands, super-resolution imaging was used to measure the kinetics of fluorescently-labeled variants to determine the impact of labeling on hybridization of the same 11-mer target DNA to the same immobilized probe DNA, on the same substrate, and under the same conditions. We measured hybridization kinetics of five fluorescently labeled targets having an identical 11-mer recognition sequence as the unlabeled target above, but with different fluorescent labels on the 5' terminus. These include labels available as phosphoramidite reagents for direct attachment during solid-phase DNA synthesis, Cy3 and carboxytetramethyl rhodamine (TAMRA), and an amine-reactive Alexa Fluor 532 (AF532) label attached to a 5' hexylamine modifier on the DNA (see Figure S1). We also compared different tethers linking a Cy3 label to the 11-mer DNA: a flexible 6-unit PEG tether and a rigid-18 base-pair double-stranded DNA tether. Hybridization kinetics were measured for labeled targets in a similar manner to the tracer (only) hybridization experiment described above. Because of the longer dissociation times of the 11-mer labeled targets (>60 sec), however, time-lapse imaging on longer (2-4s) time intervals and oxygen-scavenging enzyme buffer[35-38] were employed to reduce photobleaching and photoblinking (see Supporting Information).

The dissociation and association rates of all five dye-labeled 11-mer targets are plotted versus their solution concentrations of the corresponding target DNA in Supporting Information Figures S10 and S11. The resulting rate constants, k^o_{off} and k^o_{on}, and association constants, $K_a = k^o_{on}/k^o_{off}$, for the unlabeled and five labeled 11-mer targets are plotted in Figure 5, with numerical results tabulated in Supporting Information Table S3. All of the dye labels significantly impact the *association constant* compared to the unlabeled strand hybridization, by reducing both k^o_{on} and k^o_{off}. The Cy3 label has the greatest impact on the K_a, increasing it by 3.4-fold compared to the unlabeled strand, which is consistent with equilibrium-based competitive hybridization measurements on a similar 10-mer duplex[21] and melting assays on labeled DNA.[20] The increase in stability is due to a significantly slower k^o_{off}, while k^o_{on} is only reduced ~6% compared to the unlabeled target. Comparison of the duplex dissociation rates of Cy3-labeled versus unlabeled DNA by surface-plasmon resonance showed similar trends, with a significantly slower dissociation of the Cy3-labeled strand.[13] Molecular dynamics simulations indicate that Cy3 has strong pi-

stacking interactions with the terminal base-pair of the duplex, adding stability comparable to that of another base-pair interaction by increasing the barrier to dissociation.[18] Structurally-specific interactions between Cy3 dye labels and dsDNA have been found to impact emission yields and used to probe the dynamics of hairpin hybridization.[19]

The association equilibrium constant for hybridization of the TAMRA-labeled target is only 60% higher than that of the unlabeled target, which is consistent with previous work showing TAMRA's relatively small impact on duplex DNA melting temperatures.[49] Melting experiments, however, do not reveal the impact of a dye label on the hybridization kinetics. Although the change in duplex stability is small, TAMRA significantly slows *both* k^o_{on} and k^o_{off} by 3.5 and 5.4-fold, respectively, indicating a significant increase in the transition-state barrier to both hybridization and dissociation. Fluorescence lifetime and quenching assays indicate that TAMRA interacts with guanosine,[17,50,51] of which there are three in the target sequence. These intramolecular TAMRA-guanine interactions, which could impact both single-strand DNA structure and duplex stability, appear to increase the energy barrier to both duplex formation and dissociation, slowing both k^o_{on} and k^o_{off} with a resulting small net change in K_a.

Like TAMRA, AF532 increases the association constant K_a by less than a factor two (80%) compared to the unlabeled target strand. However, AF532 has a significantly smaller impact on the kinetics of duplex formation and dissociation: k^o_{on} is reduced by only 20%, and k^o_{off} is reduced by 50%. This suggests that AF532 does not interact as strongly with DNA as TAMRA or Cy3. Although the chromophore of AF532 is similar to TAMRA, its sulfonated structure is engineered to reduce interactions with other dyes and increase water solubility through the addition of anionic sulfonate groups.[52] Sulfonation of other dye labels has been shown to decrease their interactions and stabilization of duplex DNA,[13,50] presumably through electrostatic repulsion with the backbone phosphate groups. The longer linker on the AF532 label, from the succinimidyl ester conjugation to a terminal amine-modifier (see Figure S1), may also contribute to a reduction of the impact of the label. Of the three labels tested, AF532 presents the best choice for applications where the behavior of labeled oligos needs to match unlabeled species since it has the smallest combined impact on the kinetics and thermodynamics of duplex formation. Labeling effects on duplex stability are, however, sensitive to DNA sequence,[53] and especially the identity of the terminal base pair,[18,20] so these conclusions may not apply to all applications and DNA sequences.

To determine whether longer spacers could mitigate DNA:dye-label interactions, we also investigated DNA with two different tethers between the Cy3 label and the 5' end: a flexible 6-unit PEG spacer and a more rigid 18-base-pair double-stranded DNA segment (Figure S1). The dsDNA-linker has a Cy3 label on the 5' end of an 18-mer oligonucleotide hybridized to a complementary 18-nucleotide segment on the 5' end of the target sequence. This segment has a high melting temperature, ~59°C,[54] to ensure the duplex remains hybridized at the working temperature of 25°C. As shown in Figure 5 and Table S3, the PEG tether did not affect the K_a; it slightly reduced k^o_{on} and k^o_{off} by ~16% compared to the Cy3-target with no spacer. The PEG spacer is expected to be flexible, and it appears to present no barrier to Cy3 interactions with the single-stranded DNA target or the duplex. This result is consistent with duplex DNA melting data that showed a relatively small 1°C change in melting temperature with the addition of the same 6-unit PEG spacer between the 5' terminus and a Cy3 label.[49] In contrast, the dsDNA linker significantly alters the duplex stability compared to the proximately-bound Cy3 target: the K_a is reduced by a factor of 12 as a result of a 5-fold reduction to k^o_{on} and a 2.5-fold increase in k^o_{off}. This k^o_{off} is within 30% of the dissociation rate of unlabeled target, which suggests that the rigid linker prevents Cy3 from interacting with and stabilizing the duplex. However, k^o_{on} is greatly reduced compared to both the Cy3-labeled and unlabeled targets. This tether increases the molecular weight of the target DNA by ~4-fold, which would reduce the rate of successful hybridization by slowing the diffusion coefficient and corresponding collision frequency and by reducing the relative area of the reactive single-stranded region of the target and increasing steric hindrance.[55] These results indicate that highly flexible linkers are not able to prevent the stabilizing effects of dye labels, and while rigid dsDNA linkers can prevent these interactions, they come with a significant cost of reducing the association rate.

CONCLUSIONS

In this work, we have demonstrated a single-molecule fluorescence competitive assay at individual DNA probe sites to measure the hybridization kinetics of *unlabeled oligonucleotides*. This methodology provides a unique single-molecule approach to acquiring information on fundamental rates of DNA hybridization, free of the impact of fluorescent labels. Hybridization kinetics were determined by measuring how an unlabeled DNA target affects intervals between hybridization events of a labeled tracer DNA competing for individual probe-DNA molecules

immobilized on a surface. A rate model was developed to predict how unlabeled target DNA alters the distribution of time intervals between labeled-tracer DNA hybridization events, and the model was used to extract association and dissociation rates of the unlabeled target DNA. The predicted rate constants are consistent with the competitive equilibrium response determined by measuring the average hybridized fraction of probe DNA with tracer DNA at varying concentrations of competing target DNA. Similar analysis of single-molecule binding intervals has been used to correct association rates to account for incomplete labeling of target molecules.[56] This previous analysis, however, required identical rate constants for the labeled and unlabeled species. As the present results show, labels can significantly impact hybridization kinetics, necessitating an analysis that allows for unique rates for each species.

Comparing the hybridization rate constants of labeled and unlabeled DNA shows that the fluorescent labels attached directly to the terminal base pair decrease the dissociation rate by factors of 2-5, and decrease the association rate by as much as a factor of 3.5. Attaching the fluorescent label by means a flexible PEG tether does little to reduce the impact of a dye label; a rigid dsDNA tether, however, nearly eliminates the label impact on the dissociation rate but at a cost of much slower association due to the size of the tether. These results are generally consistent with previous equilibrium measurements of the impact of dye labeling on the duplex association constant. In some cases, an apparently small change in association constant masks the significant but proportional changes in association and dissociation rates. The present work allows us to measure and compare the kinetics and association constants of labeled and unlabeled DNA hybridization under the same conditions with the same probe-strand immobilization and detection scheme. This capability could help in the selection of specific labels to minimize perturbations to the association or dissociation rates depending on the needs of the assay and the allowable label interactions, which can be sensitive to DNA sequence and structure.[18,20,53] The single-molecule competitive DNA assay could be used to determine the kinetics of other ternary DNA reactions such as analyte binding in structure-switching aptamers.[57-59] These assays often rely on the competitive association of a DNA aptamer probe strand with a labeled DNA read-out strand and an unlabeled target analyte. Intervals between hybridization of the aptamer probe with the labeled read-out strand could be employed to determine the unlabeled analyte binding kinetics, while avoiding fluorescent labeling of the analyte which could significantly alter its aptamer binding affinity.[60] In general, this measurement concept could be extended to studies of

a variety of other reversible reaction systems, where kinetics of unlabeled species can be determined from their influence on the reaction of a labeled species with localized probe molecules on a surface.

ACKNOWLEDGEMENTS

This work was supported in part by the National Science Foundation under grants CHE-1608949 and CHE-1904424. The authors thank Michael W. Manhart for his help with immobilization chemistry and Mike Hanson and the University of Utah DNA/Peptide Facility, for oligo synthesis and purification.

Supporting Information Available. Additional information is provided on the structure of the fluorescent labels, mitigating and testing for photobleaching, locating and tracking single molecules, Poisson-Erlang distributions of measured lifetimes, impact of unlabeled target DNA on tracer dissociation, Monte-Carlo simulations of hybridization intervals, covariance of rate parameters, effects of lifetime variance on reported rates, individual probe sites event statistics, tracer dissociation and association rates, competitive equilibrium analysis model, labeled 11-mer target hybridization kinetics, and an example video of 9-mer tracer imaging data. This material is available free of charge via the Internet at http://pubs.acs.org

REFERENCES

(1) Iinuma, R.; Ke, Y.; Jungmann, R.; Schlichthaerle, T.; Woehrstein, J. B.; Yin, P. Polyhedra Self-Assembled from DNA Tripods and Characterized with 3D DNA-PAINT. *Science* **2014**, *344*, 65-69.

(2) Kent, A. D.; Spiropulos, N. G.; Heemstra, J. M. General Approach for Engineering Small-Molecule-Binding DNA Split Aptamers. *Anal. Chem.* **2013**, *85*, 9916-9923.

(3) Bumgarner, R. DNA microarrays: Types, Applications and their future. *Current protocols in molecular biology / edited by Frederick M. Ausubel ... [et al.]* **2013**, *0 22*, Unit-22.21.

(4) Carthew, R. W.; Sontheimer, E. J. Origins and Mechanisms of miRNAs and siRNAs. *Cell*, *136*, 642-655.

(5) Morrison, L. E.; Stols, L. M. Sensitive fluorescence-based thermodynamic and kinetic measurements of DNA hybridization in solution. *Biochemistry* **1993**, *32*, 3095-3104.

(6) Watterson, J. H.; Piunno, P. A. E.; Wust, C. C.; Krull, U. J. Effects of Oligonucleotide Immobilization Density on Selectivity of Quantitative Transduction of Hybridization of Immobilized DNA. *Langmuir* **2000**, *16*, 4984-4992.

(7) Jungmann, R.; Steinhauer, C.; Scheible, M.; Kuzyk, A.; Tinnefeld, P.; Simmel, F. C. Single-Molecule Kinetics and Super-Resolution Microscopy by Fluorescence Imaging of Transient Binding on DNA Origami. *Nano Lett.* **2010**, *10*, 4756-4761.

(8) Kastantin, M.; Schwartz, D. K. Connecting Rare DNA Conformations and Surface Dynamics Using Single-Molecule Resonance Energy Transfer. *ACS Nano* **2011**, *5*, 9861-9869.

(9) Dupuis, Nicholas F.; Holmstrom, Erik D.; Nesbitt, David J. Single-Molecule Kinetics Reveal Cation-Promoted DNA Duplex Formation Through Ordering of Single-Stranded Helices. *Biophys. J.* **2013**, *105*, 756-766.

(10) Kastantin, M.; Schwartz, D. K. DNA Hairpin Stabilization on a Hydrophobic Surface. *Small* **2013**, *9*, 933-941.

(11) Monserud, J. H.; Schwartz, D. K. Mechanisms of Surface-Mediated DNA Hybridization. *ACS Nano* **2014**, *8*, 4488-4499.

(12) Johnson-Buck, A.; Su, X.; Giraldez, M. D.; Zhao, M.; Tewari, M.; Walter, N. G. Kinetic fingerprinting to identify and count single nucleic acids. *Nat Biotech* **2015**, *33*, 730-732.

(13) Sobek, J.; Rehrauer, H.; Schauer, S.; Fischer, D.; Patrignani, A.; Landgraf, S.; Korlach, J.; Schlapbach, R. Single-molecule DNA hybridisation studied by using a modified DNA sequencer: a comparison with surface plasmon resonance data. *Methods and Applications in Fluorescence* **2016**, *4*, 015002.

(14) Su, X.; Li, L.; Wang, S.; Hao, D.; Wang, L.; Yu, C. Single-Molecule Counting of Point Mutations by Transient DNA Binding. *Sci. Rep.* **2017**, *7*, 43824.

(15) Yazawa, K.; Furusawa, H. Probing Multiple Binding Modes of DNA Hybridization: A Comparison between Single-Molecule Observations and Ensemble Measurements. *ACS Omega* **2018**, *3*, 2084-2092.

(16) Schreiner, S. M.; Hatch, A. L.; Shudy, D. F.; Howard, D. R.; Howell, C.; Zhao, J.; Koelsch, P.; Zharnikov, M.; Petrovykh, D. Y.; Opdahl, A. Impact of DNA–Surface Interactions on the Stability of DNA Hybrids. *Anal. Chem.* **2011**, *83*, 4288-4295.

(17) Heinlein, T.; Knemeyer, J.-P.; Piestert, O.; Sauer, M. Photoinduced Electron Transfer between Fluorescent Dyes and Guanosine Residues in DNA-Hairpins. *The Journal of Physical Chemistry B* **2003**, *107*, 7957-7964.

(18) Spiriti, J.; Binder, J. K.; Levitus, M.; van der Vaart, A. Cy3-DNA Stacking Interactions Strongly Depend on the Identity of the Terminal Basepair. *Biophys. J.* **2011**, *100*, 1049-1057.

(19) Morten, M. J.; Lopez, S. G.; Steinmark, I E.; Rafferty, A.; Magennis, S. W. Stacking-induced fluorescence increase reveals allosteric interactions through DNA. *Nucleic Acids Res.* **2018**, *46*, 11618-11626.

(20) Moreira, B. G.; You, Y.; Owczarzy, R. Cy3 and Cy5 dyes attached to oligonucleotide terminus stabilize DNA duplexes: Predictive thermodynamic model. *Biophys. Chem.* **2015**, *198*, 36-44.

(21) Peterson, E. M.; Manhart, M. W.; Harris, J. M. Competitive Assays of Label-Free DNA Hybridization with Single-Molecule Fluorescence Imaging Detection. *Anal. Chem.* **2016**, *88*, 6410-6417.

(22) Okahata, Y.; Kawase, M.; Niikura, K.; Ohtake, F.; Furusawa, H.; Ebara, Y. Kinetic Measurements of DNA Hybridization on an Oligonucleotide-Immobilized 27-MHz Quartz Crystal Microbalance. *Anal. Chem.* **1998**, *70*, 1288-1296.

(23) Peterlinz, K. A.; Georgiadis, R. M.; Herne, T. M.; Tarlov, M. J. Observation of Hybridization and Dehybridization of Thiol-Tethered DNA Using Two-Color Surface Plasmon Resonance Spectroscopy. *J. Am. Chem. Soc.* **1997**, *119*, 3401-3402.

(24) Li, Z.; Weeraman, C. N.; Azam, M. S.; Osman, E.; Gibbs-Davis, J. M. The thermal reorganization of DNA immobilized at the silica/buffer interface: a vibrational sum frequency generation investigation. *PCCP* **2015**, *17*, 12452-12457.

(25) Lei, Q.-l.; Ren, C.-l.; Su, X.-h.; Ma, Y.-q. Crowding-induced Cooperativity in DNA Surface Hybridization. *Scientific Reports* **2015**, *5*, 9217.

(26) Peterson, A. W.; Heaton, R. J.; Georgiadis, R. M. The effect of surface probe density on DNA hybridization. *Nucleic Acids Res.* **2001**, *29*, 5163-5168.

(27) Michel, W.; Mai, T.; Naiser, T.; Ott, A. Optical Study of DNA Surface Hybridization Reveals DNA Surface Density as a Key Parameter for Microarray Hybridization Kinetics. *Biophys. J.* **2007**, *92*, 999-1004.

(28) Goldstein, B.; Coombs, D.; He, X.; Pineda, A. R.; Wofsy, C. The influence of transport on the kinetics of binding to surface receptors: application to cells and BIAcore. *J. Mol. Recognit.* **1999**, *12*, 293-299.

(29) Chen, J.; Bremauntz, A.; Kisley, L.; Shuang, B.; Landes, C. F. Super-Resolution mbPAINT for Optical Localization of Single-Stranded DNA. *ACS Appl. Mater. Interfaces* **2013**, *5*, 9338-9343.

(30) Peterson, E. M.; Harris, J. M. Identification of Individual Immobilized DNA Molecules by Their Hybridization Kinetics Using Single-Molecule Fluorescence Imaging. *Anal. Chem.* **2018**, *90*, 5007-5014.

(31) Mao, X.; Liu, C.; Hesari, M.; Zou, N.; Chen, P. Super-resolution imaging of non-fluorescent reactions via competition. *Nature Chemistry* **2019**, *11*, 687-694.

(32) Kern, W.; Poutinen, D. A. Cleaning solution based on hydrogen peroxide for use in silicon semiconductor technology. *RCA Review* **1970**, *31*, 9.

(33) Tsukruk, V. V.; Luzinov, I.; Julthongpiput, D. Sticky Molecular Surfaces: Epoxysilane Self-Assembled Monolayers. *Langmuir* **1999**, *15*, 3029-3032.

(34) Jung, G.-Y.; Li, Z.; Wu, W.; Chen, Y.; Olynick, D. L.; Wang, S.-Y.; Tong, W. M.; Williams, R. S. Vapor-Phase Self-Assembled Monolayer for Improved Mold Release in Nanoimprint Lithography. *Langmuir* **2005**, *21*, 1158-1161.

(35) Shi, X.; Lim, J.; Ha, T. Acidification of the Oxygen Scavenging System in Single-Molecule Fluorescence Studies: In Situ Sensing with a Ratiometric Dual-Emission Probe. *Anal. Chem.* **2010**, *82*, 6132-6138.

(36) Aitken, C. E.; Marshall, R. A.; Puglisi, J. D. An Oxygen Scavenging System for Improvement of Dye Stability in Single-Molecule Fluorescence Experiments. *Biophys. J.*, *94*, 1826-1835.

(37) Cordes, T.; Vogelsang, J.; Tinnefeld, P. On the Mechanism of Trolox as Antiblinking and Antibleaching Reagent. *J. Am. Chem. Soc.* **2009**, *131*, 5018-5019.

(38) Glembockyte, V.; Lincoln, R.; Cosa, G. Cy3 Photoprotection Mediated by Ni2+ for Extended Single-Molecule Imaging: Old Tricks for New Techniques. *J. Am. Chem. Soc.* **2015**, *137*, 1116-1122.

(39) Robbins, M. S.; Hadwen, B. J. The noise performance of electron multiplying charge-coupled devices. *IEEE Trans. Electron Devices* **2003**, *50*, 1227-1232.

(40) Peterson, E. M.; Harris, J. M. Quantitative Detection of Single Molecules in Fluorescence Microscopy Images. *Anal. Chem.* **2010**, *82*, 189-196.

(41) Jungmann, R.; Avendano, M. S.; Dai, M.; Woehrstein, J. B.; Agasti, S. S.; Feiger, Z.; Rodal, A.; Yin, P. Quantitative super-resolution imaging with qPAINT. *Nat Meth* **2016**, *13*, 439-442.

(42) Gooding, J. J.; Gaus, K. Single-Molecule Sensors: Challenges and Opportunities for Quantitative Analysis. *Angew. Chem. Int. Ed.* **2016**, *55*, 11354-11366.

(43) Johnson-Buck, A.; Li, J.; Tewari, M.; Walter, N. G. A guide to nucleic acid detection by single-molecule kinetic fingerprinting. *Methods* **2019**, *153*, 3-12.

(44) Walder, R.; Kastantin, M.; Schwartz, D. K. High throughput single molecule tracking for analysis of rare populations and events. *Analyst* **2012**, *137*, 2987-2996.

(45) Hall, P.; Selinger, B. Better estimates of exponential decay parameters. *J. Phys. Chem.* **1981**, *85*, 2941-2946.

(46) Krishnamoorthy, K. In *Handbook of Statistical Distributions with Applications, Second Edition*; Chapman and Hall/CRC: 2015, p 215-245.

(47) Zhang, D. Y.; Winfree, E. Control of DNA Strand Displacement Kinetics Using Toehold Exchange. *J. Am. Chem. Soc.* **2009**, *131*, 17303-17314.

(48) Myers, G. A.; Gacek, D. A.; Peterson, E. M.; Fox, C. B.; Harris, J. M. Microscopic Rates of Peptide–Phospholipid Bilayer Interactions from Single-Molecule Residence Times. *J. Am. Chem. Soc.* **2012**, *134*, 19652-19660.

(49) Moreira, B. G.; You, Y.; Behlke, M. A.; Owczarzy, R. Effects of fluorescent dyes, quenchers, and dangling ends on DNA duplex stability. *Biochem. Biophys. Res. Commun.* **2005**, *327*, 473-484.

(50) Ranjit, S.; Levitus, M. Probing the Interaction Between Fluorophores and DNA Nucleotides by Fluorescence Correlation Spectroscopy and Fluorescence Quenching†. *Photochem. Photobiol.* **2012**, *88*, 782-791.

(51) Chen, T.; Fu, L.; Zu, L. Steady-state and time-resolved fluorescence of tetramethylrhodamine attached to DNA: correlation with DNA sequences. *Luminescence* **2013**, *28*, 860-864.

(52) Panchuk-Voloshina, N.; Haugland, R. P.; Bishop-Stewart, J.; Bhalgat, M. K.; Millard, P. J.; Mao, F.; Leung, W.-Y.; Haugland, R. P. Alexa Dyes, a Series of New Fluorescent Dyes that Yield Exceptionally Bright, Photostable Conjugates. *Journal of Histochemistry & Cytochemistry* **1999**, *47*, 1179-1188.

(53) Kretschy, N.; Somoza, M. M. Comparison of the Sequence-Dependent Fluorescence of the Cyanine Dyes Cy3, Cy5, DyLight DY547 and DyLight DY647 on Single-Stranded DNA. *PLoS ONE* **2014**, *9*, e85605.

(54) Owczarzy, R.; You, Y.; Moreira, B. G.; Manthey, J. A.; Huang, L.; Behlke, M. A.; Walder, J. A. Effects of Sodium Ions on DNA Duplex Oligomers: Improved Predictions of Melting Temperatures. *Biochemistry* **2004**, *43*, 3537-3554.

(55) Šolc, K.; Stockmayer, W. H. Kinetics of diffusion-controlled reaction between chemically asymmetric molecules. II. Approximate steady-state solution. *Int. J. Chem. Kinet.* **1973**, *5*, 733-752.

(56) Li, Y.; Augustine, G. J.; Weninger, K. Kinetics of Complexin Binding to the SNARE Complex: Correcting Single Molecule FRET Measurements for Hidden Events. *Biophys. J.* **2007**, *93*, 2178-2187.

(57) Nutiu, R.; Li, Y. Structure-Switching Signaling Aptamers. *J. Am. Chem. Soc.* **2003**, *125*, 4771-4778.

(58) Yang, K.-A.; Chun, H.; Zhang, Y.; Pecic, S.; Nakatsuka, N.; Andrews, A. M.; Worgall, T. S.; Stojanovic, M. N. High-Affinity Nucleic-Acid-Based Receptors for Steroids. *ACS Chemical Biology* **2017**, *12*, 3103-3112.

(59) Chen, J.; Fang, Z.; Liu, J.; Zeng, L. A simple and rapid biosensor for ochratoxin A based on a structure-switching signaling aptamer. *Food Control* **2012**, *25*, 555-560.

(60) Elenko, M. P.; Szostak, J. W.; van Oijen, A. M. Single-Molecule Imaging of an in Vitro-Evolved RNA Aptamer Reveals Homogeneous Ligand Binding Kinetics. *J. Am. Chem. Soc.* **2009**, *131*, 9866-9867.

FIGURES AND SCHEMES

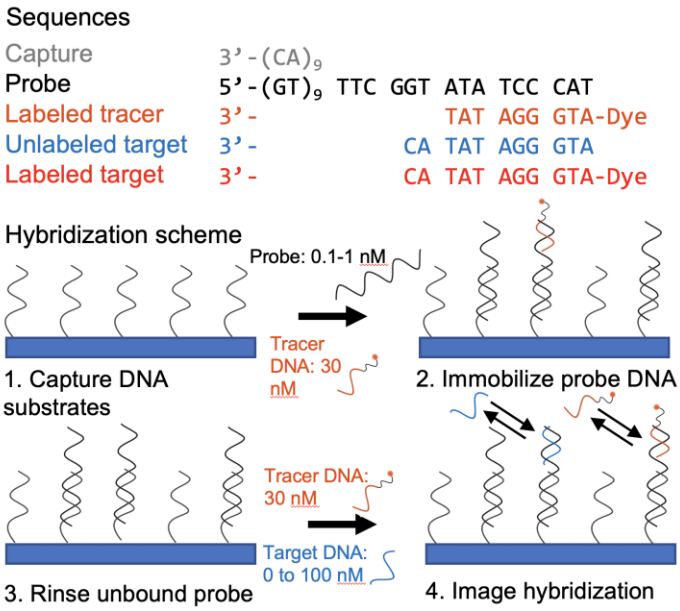

Scheme 1. DNA sequences and hybridization. Upper: Sequences of capture, probe, tracer, unlabeled, and labeled target DNA. Lower: Hybridization scheme showing:
1. Injection of mixture of probe and tracer DNA; 2. Capture of probes at surface monitored using tracer DNA; 3. Rinsing to remove uncaptured probe; and 4. Injection of solutions of tracer and unlabeled target to measure hybridization kinetics.

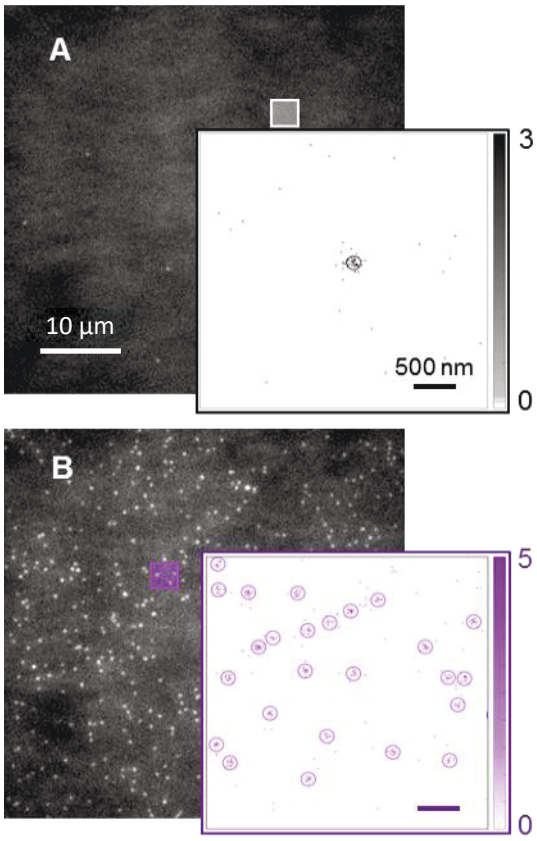

Figure 1. Hybridization selectivity for tracer DNA binding to probe DNA. A) Image of 30-nM tracer DNA over a blank surface with capture strands but no probe; B) after probe immobilization. Insets: histogram maps of events with located probe sites.

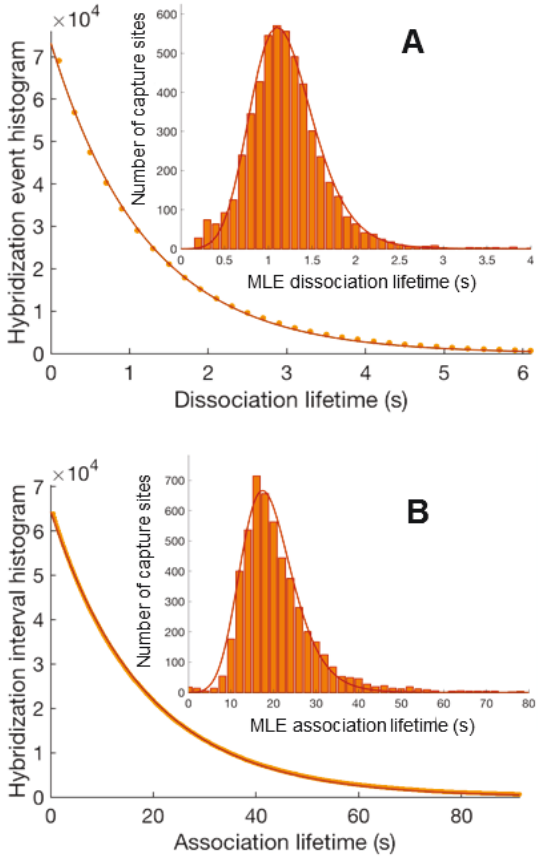

Figure 2. Hybridization kinetics of tracer DNA. A) Histograms of dissociation lifetimes and B) association times. Insets: probe-site distribution of MLE of dissociation lifetimes (A) and association lifetimes (B) with calculated Poisson-Erlang distributions.

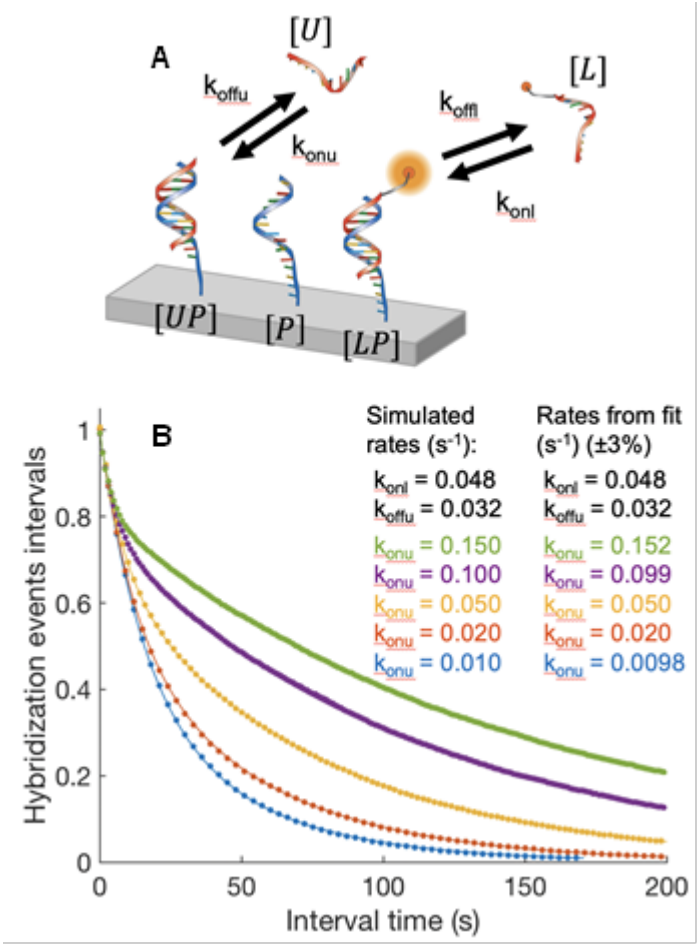

Figure 3. Monte-Carlo simulations of competitive hybridization. A) Hybridization model with rates and concentra-tions defined. B) Hybridization intervals from simulation (points) fit to Equations 6 (lines); Inset: rates used in the simulation (left) and rates determined from fit.

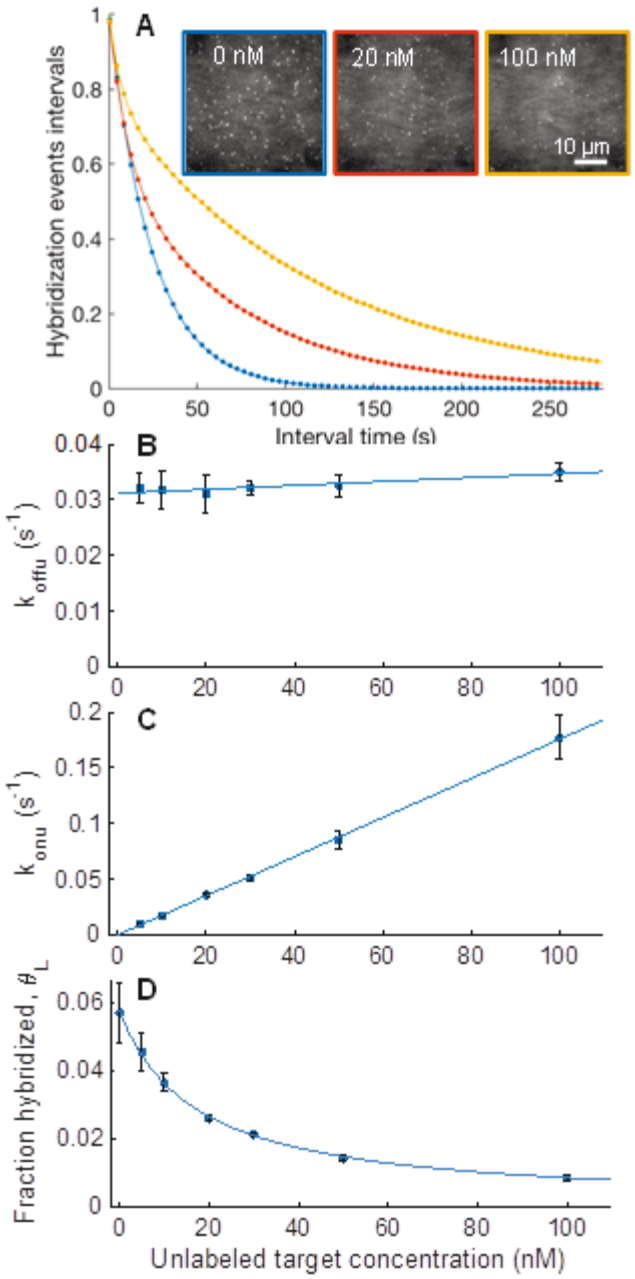

Figure 4. Hybridization kinetics of the unlabeled target. A) Interval histograms for 30-nM tracer DNA with 0 (blue), 20-nM (orange), and 100-nM (yellow) unlabeled target DNA (points), with fits to Equation 6 (lines). B) Plot of dissociation rate of unlabeled target DNA from fits above with a linear least-squares fit having a slope indistinguishable from zero at 95% confidence. C) Association rates with linear least squares fit with zero intercept (line). D) Fraction of sites hybridized with tracer calculated from average lifetimes with fit to Equation 13 (line).

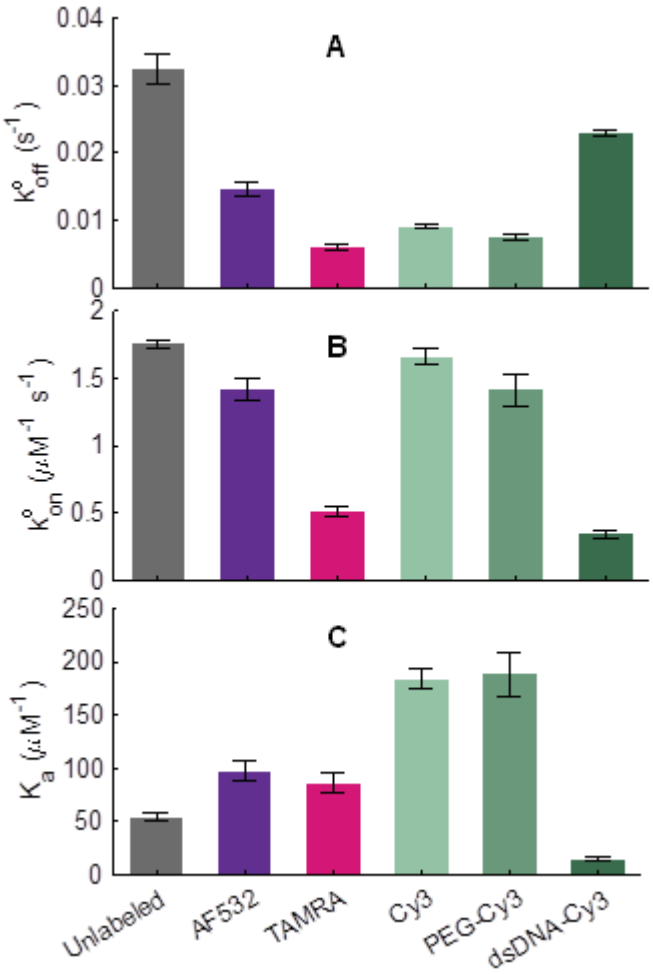

Figure 5: Hybridization kinetic rate constants of 5' fluorescently modified target DNA: A) dissociation rate constant, k^o_{off}, B) association rate constant, k^o_{on}, and C) association constant, K_a. Labeled targets kinetics were measured by molecule tracking, and unlabeled target kinetics were measured using competitive hybridization scheme. Error bars are 2 standard deviations of the mean.

TOC Graphic

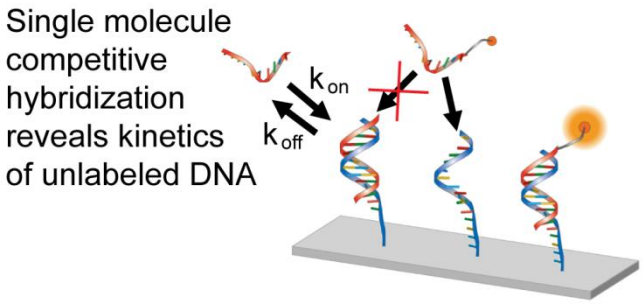
Single molecule
competitive
hybridization
reveals kinetics
of unlabeled DNA
k on
k off